Chinese Chemical Letters 36 (2025) 110561

Contents lists available at ScienceDirect

Chinese Chemical Letters

journal homepage: www.elsevier.com/locate/cclet

Online detecting living cells released TNF-α and studying intercellular communication using SuperDNA self-assembled conical nanochannel

Weiwei Liu[a], Yu Liu[a], Zhaoyan Tian[b], Zhaohan Wang[a], Hui Liu[a], Songqin Liu[a], Yafeng Wu[a,*]

[a] *Jiangsu Engineering Laboratory of Smart Carbon-Rich Materials and Device, School of Chemistry and Chemical Engineering, Southeast University, Nanjing 211189, China*

[b] *State Key Laboratory for Macromolecule Drugs and Large-scale Manufacturing, School of Pharmaceutical Sciences, Liaocheng University, Liaocheng 252059, China*

ARTICLE INFO

Article history:
Received 23 June 2024
Revised 23 September 2024
Accepted 17 October 2024
Available online 18 October 2024

Keywords:
Nanochannel
Ion transport
In situ detection
Cell secretions
Intercellular communication

ABSTRACT

Nanochannel technology based on ionic current rectification has emerged as a powerful tool for the detection of biomolecules owing to unique advantages. Nevertheless, existing nanochannel sensors mainly focus on the detection of targets in solution or inside the cells, moreover, they only have a single function, greatly limiting their application. Herein, we fabricated SuperDNA self-assembled conical nanochannel, which was clamped in the middle of self-made device for two functions: Online detecting living cells released TNF-α and studying intercellular communication. Polyethylene terephthalate (PET) membrane incubated tumor associated macrophages and tumor cells was rolled up and inserted into the left and right chamber of the device, respectively. Through monitoring the ion current change in the nanochannel, tumor associated macrophages released TNF-α could be *in situ* and noninvasive detected with a detection limit of 0.23 pg/mL. Furthermore, the secreted TNF-α induced epithelial-mesenchymal transformation of tumor cells in the right chamber was also studied. The presented strategy displayed outstanding performance and multi-function, providing a promising platform for *in situ* non-destructive detection of cell secretions and related intercellular communication analysis.

Tumor associated macrophages (TAMs) are an important component of the tumor microenvironment, and the interaction between tumor cells and macrophages is of great significance in the proliferation, metastasis, invasion, and immune processes of tumors [1-3]. The secretion of cytokines reflects the complex mechanism of tumor-macrophage interaction, for example, TAMs secreted tumor necrosis factor-α (TNF-α) is one of the key molecules mediating the inflammatory process and promoting tumor growth [4]. High dose local administration of TNF-α has strong tumor necrosis activity, while low dose chronic production may participate in all steps of tumorigenesis as an endogenous tumor promoter, including cell transformation, proliferation, growth, invasion, angiogenesis and metastasis [5,6], which always accompanied with epithelial-mesenchymal transition (EMT) [7,8]. Therefore, it is crucial to real time monitor the TAMs released TNF-α level and to further investigate the intercellular communication between tumor cells and macrophages.

The traditional detection methods for cytokines are fluorescence [9,10], enzyme-linked immunosorbent assay (ELISA) and mass spectrometry [11-13]. They encountered some bottleneck problems in the development process, on the one hand, the requirement to label the target analytes, cumbersome operation, long analysis time, which inevitably caused cell damage; on the other hand, channel interface performance and analysis devices were difficult to meet the needs of *in situ* non-destructive analysis of low-abundance cell secretions [14-16].

Nowadays, nanochannel technology based on ionic current rectification (ICR) has emerged as a powerful tool for the detection of biomolecules owing to the unique advantages, such as label-free, simple sample process, high-spatial and temporal resolution and high sensitivity [17-22]. Different from traditional electrochemical analysis methods, which take physical quantities such as electrode potential, electric quantity, current voltage and conductance as response signals, this technology reflects the quantity change of target analyte with the change of ICR [23,24]. ICR refers to the asymmetric ion current response under bias in different directions, similar to diodes in electronics [25]. Asymmetric factors in the nanochannel such as structural asymmetry, surface charge distribu-

* Corresponding author.
E-mail address: wuyafeng@seu.edu.cn (Y. Wu).

https://doi.org/10.1016/j.cclet.2024.110561
1001-8417/

tion asymmetry, concentration distribution asymmetry lead to the asymmetric concentration distribution of cations and ions in the channel [26-29]. For example, Xia's group introduced supersandwich DNA probes (SSW-DNA) on the outer surface of nanochannels with hydrophobic inner walls, enabling reliable on-site qualitative detection and ultra-sensitive quantitative analysis of microcystin-leucine arginine (MC-LR) [30]. Liu's group designed artificial hydrogen peroxide (H_2O_2)-activated nanochannels by decorating the inner pore surface with 4-(phenoxymethyl)benzeneboronic acid pinacol ester (PBAE), exhibiting a highly selective and sensitive response toward H_2O_2 [31]. Xu's group combined the ionic current rectification property of nanopipette reactor with duplex specific nuclease-assisted hybridization chain reaction for signal amplification to realize ultrasensitive intracellular miR-10b analysis [23]. Existing nanochannel sensors mainly focus on the detection of targets in solution or inside the cells, while *in situ* analysis of biomolecules outside the cells are rarely reported. Moreover, most nanochannel sensors only have a single function, limiting their capacity to meet the diverse requirements of multi-faceted sensing systems.

In this work, we fabricated SuperDNA self-assembled conical nanochannel for online detecting living cells released TNF-α and studying intercellular communication (Scheme 1). SuperDNA nanostructures were self-assembled on the tip side of conical nanochannel with the diameter of 137 nm through hybridization chain reaction (HCR). Then the modified nanochannel was clamped in the middle of the self-made device, where polyethylene terephthalate (PET) membrane incubated tumor associated macrophages (differentiated U937) was rolled up and inserted into the left chamber; PET membrane incubated tumor cells (BxPC-3) was rolled up and inserted into the right chamber. Lipopolysaccharides (LPS) was added in the left chamber to stimulate U937 cells to secrete TNF-α, which opened the SuperDNA structure. Through monitoring the ion current change in the nanochannel, living cells released TNF-α could be *in situ* and noninvasive detected. We achieved a reliable detection limit of 0.23 pg/mL for TNF-α. In addition, the TNF-α mediated intercellular communication between tumor associated macrophages (U937) and tumor cells (BxPC-3) was also investigated. TNF-α induced epithelial-mesenchymal transformation of BxPC-3 cells, which confirmed by down-regulated EMT marker E-cadherin and up-regulated vimentin. Therefore, the proposed platform is expected to be a promising tool for studying cytokines mediated intercellular communication.

The PET nanochannel was fabricated according to surfactant-assisted ion-track etching method [32]. Scanning electron microscope (SEM) images clearly exhibited the asymmetric conical structure of the fabricated nanochannel (Fig. 1A, Fig. S1 in Supporting information), the diameter of the base side and tip side was about 2.6 μm and 137 nm, respectively. For self-assembling SuperDNA in the nanochannel, Au was firstly sputtered from tip side (PET-Au), then capture probe (CP) DNA was anchored on the surface through Au-S bonds (PET-Au-CP), following that P1 and P2 were introduced to trigger HCR process to obtain SuperDNA modified nanochannel (PET-Au-SuperDNA) [33,34]. The formation of SuperDNA was verified by gel electrophoresis (Fig. 1B), the length of SuperDNA was maximum, reaching >2000 base pairs, much larger than the length of Marker, P1 and P2. The base sequences of each DNA strand were shown in Table S1 (Supporting information) and the structure of SuperDNA was shown in Fig. S2 (Supporting information). In order to further prove the successful construction of PET-Au-SuperDNA, surface contact angle and corresponding X-ray Photoelectron spectroscopy (XPS) characterization of PET, PET-Au and PET-Au-SuperDNA were performed. The contact angles of PET, PET-Au and PET-Au-SuperDNA were presented in Fig. 1C, compared with PET and PET-Au, PET-Au-SuperDNA exhibited increased hydrophilicity due to the introduction of SuperDNA nanostructures. XPS pattern showed that there was a characteristic peak of Au 4f for PET-Au and a characteristic peak of N 1s for PET-Au-SuperDNA (Fig. 1D). All above results demonstrated the successful preparation of PET-Au-SuperDNA.

The ion transport properties of the prepared nanochannel were studied by self-made electrochemical cell (Fig. S3 in Supporting information). The Au coated PET nanochannel (PET-Au) displayed a diode-like *I-V* curve with the ICR ratio ($|I_{-2V}|/I_{+2V}$) of 25.03, after the modification of SuperDNA (PET-Au-SuperDNA), the $|I_{-2V}|/I_{+2V}$ decreased from 25.03 to 3.43, ascribing that the tip side was significantly blocked by SuperDNA nanostructures. SuperDNA nanostructures contained aptamer sequence for cell secretion TNF-α, thus after the addition of TNF-α, SuperDNA nanostructures collapsed and opened the tip side, the $|I_{-2V}|/I_{+2V}$ retrieved to 70.52% of that measured in PET-Au, demonstrating the feasibility of quantitatively detecting TNF-α (Fig. 2A). Due to the introduction of cy5 group at the 3′ end of DNA aptamer, the modified state can also be

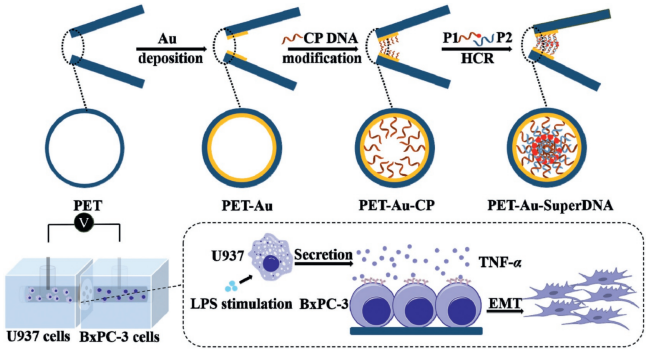

Scheme 1. Schematic illustration of *in situ* non-destructive detection of cell secretion TNF-α based on confined ion transport and investigation of intercellular communication. PET: polyethylene terephthalate; CP DNA: capture probe DNA; HCR: hybridization chain reaction; LPS: lipopolysaccharides; TNF-α: tumor necrosis factor-α; EMT: epithelial-mesenchymal transition.

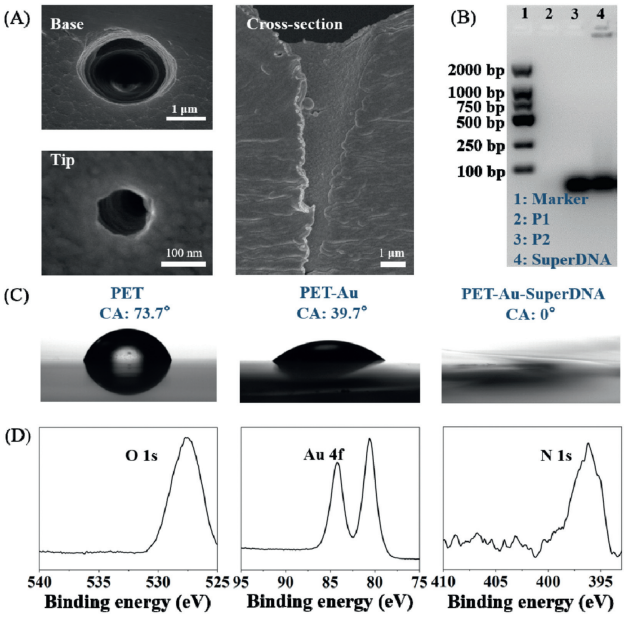

Fig. 1. Preparation and characterization of the PET-Au-SuperDNA nanochannel. (A) Scanning electron microscopy (SEM) image of the base side, tip side, and cross-section of the etched PET nanochannel. (B) Analysis of HCR products using 2% agarose gel electrophoresis. (C) Surface contact angles of PET, PET-Au and PET-Au-SuperDNA. (D) XPS spectra of PET, PET-Au and PET-Au-SuperDNA.

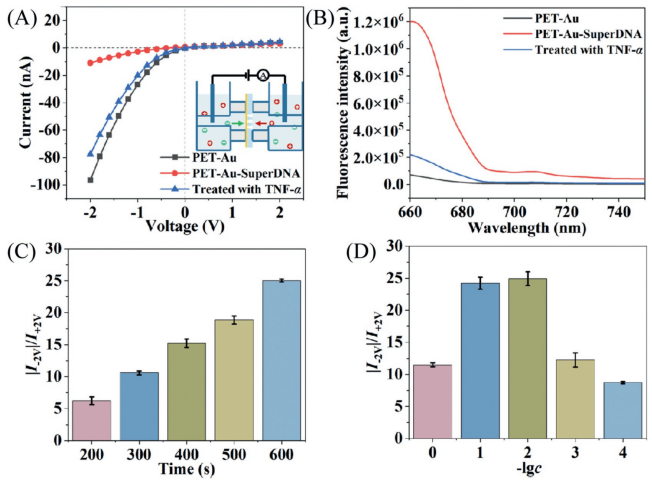

Fig. 2. (A) *I-V* plots of the PET-Au, PET-Au-SuperDNA and treated with TNF-α. Inset: section of self-made electrochemical cell. (B) Fluorescence spectrum of the PET-Au, PET-Au-SuperDNA and treated with TNF-α. (C) Optimization of Au deposition time. Error bars represent standard deviations from five repeated measurements. (D) Optimization of electrolyte solution concentration of KCl.

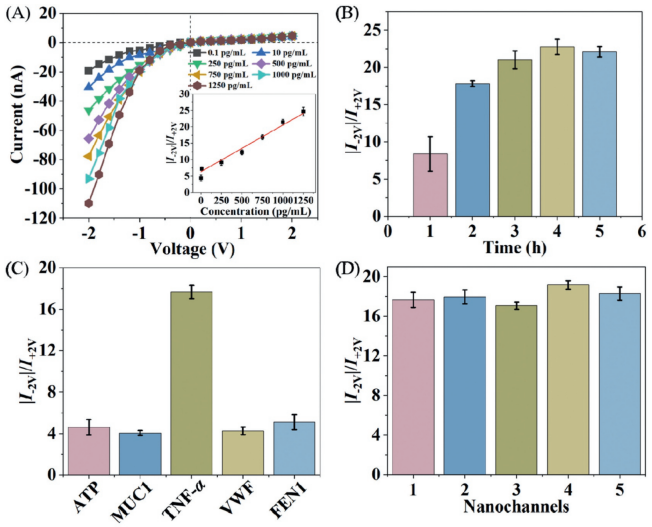

Fig. 3. (A) *I-V* properties of the nanochannel toward different TNF-α concentrations. Inset: the corresponding standard work curve. (B) Time dependence for TNF-α and PET-Au-SuperDNA. (C) Selectivity assessment of PET-Au-SuperDNA toward ATP, MUC1, TNF-α, VWF and FEN1. The concentration was 750 pg/mL. (D) The $|I_{-2V}|/I_{+2V}$ of five PET-Au-SuperDNA fabricated independently.

reflected by fluorescence spectra and laser scanning confocal microscopy (CLSM). As displayed in Fig. 2B, characteristic peak of cy5 at 667 nm was observed for PET-Au-SuperDNA, upon treatment of TNF-α, the peak disappeared. The CLSM images on the tip side of the nanochannel were consistent with the fluorescence results (Fig. S4 in Supporting information), further confirming the SuperDNA assembly and disassembly ability in the channel.

To obtain the highest $|I_{-2V}|/I_{+2V}$ for the following bioanalysis, Au deposition time and electrolyte concentration for TNF-α detection were optimized. With the prolonging of the Au deposition time, the size of tip side was reduced, further increasing the asymmetric extent of the conical nanochannel, thus the $|I_{-2V}|/I_{+2V}$ was gradually increased. When the Au deposition time was 600 s, the $|I_{-2V}|/I_{+2V}$ reached 25.03 (Fig. 2C). In addition, we observed the blockage risk of tip side increased significantly over 600 s. To investigate the effect of ion concentration on the $|I_{-2V}|/I_{+2V}$, different electrolyte concentrations of KCl at pH 7.0 were added into detection device. As shown in Fig. 2D, the $|I_{-2V}|/I_{+2V}$ increased with the increasing KCl concentration from 0.1 mmol/L to 10 mmol/L due to the accumulation and depletion of ions gradually increased, it reached a maximum value when KCl concentration tend to 10 mmol/L. At high salt solution concentration, however, the electrical double-layer at the conical nanochannel wall can powerfully shield the surface charges weakening cation-selective. Thus, the $|I_{-2V}|/I_{+2V}$ decreased with the increasing KCl concentration from 10 mmol/L to 1 mol/L. Therefore, the Au deposition time and KCl electrolyte concentration were chosen to be 600 s and 10 mmol/L for subsequent experiments, respectively.

Under the optimal conditions, *I-V* curves with different concentrations of TNF-α were recorded and shown in Fig. 3A. The current at -2 V gradually increased from 19.36 nA to -109.76 nA with the augment of TNF-α concentration from 0.1 pg/mL to 1250 pg/mL. The $|I_{-2V}|/I_{+2V}$ showed an excellent linear relationship with TNF-α concentrations. The linear regression equation was $|I_{-2V}|/I_{+2V} = 6.36 + 0.01C$ ($R^2 = 0.97$) with the detection limit (LOD) of 0.23 pg/mL, it was lower than other reported methods (Table S2 in Supporting information). About the time dependence for the TNF-α and PET-Au-SuperDNA, the $|I_{-2V}|/I_{+2V}$ gradually increased with the extension of incubation time, and tended to be stable after 4 h, suggesting that TNF-α had fully reacted with SuperDNA (Fig. 3B). To evaluate the specificality of PET-Au-SuperDNA for TNF-α, other interference species (ATP, MUC1, VWF and VEGF) were used to replace TNF-α. TNF-α treated PET-Au-SuperDNA exhibited significantly higher $|I_{-2V}|/I_{+2V}$ than other species treated nanochannel (Fig. 3C), indicating its good specificity. The $|I_{-2V}|/I_{+2V}$ of five PET-Au-SuperDNA fabricated independently confirmed a good repeatability (Fig. 3D). The stability of the fabricated PET-Au-SuperDNA was evaluated through assessments of intra-assay ($n = 5$). The relative standard deviation (RSD) of intra-assays was 2.22%, representing acceptable stability. These results confirmed the feasibility of PET-Au-SuperDNA for the detection of TNF-α.

The nuclease resistance and thermal stability were important for *in situ* intracellular detection. To verify the nuclease resistance of SuperDNA nanostructures, gel electrophoresis was conducted, the SuperDNA remained in almost the same position before and after treatment with RPMI-1640 medium containing 10% fetal bovine serum (FBS) for 12 h at 37 °C (Fig. S5 in Supporting information). The transmembrane current of PET-Au-SuperDNA showed stability before and after treatment (Fig. S6 in Supporting information).

These results confirmed that PET-Au-SuperDNA has excellent serum resistance and thermal stability, which could be used for subsequent *in situ* cell analysis. Cells were inoculated on flexible PET, then curled and placed in the left chamber of self-made electrochemical cell (Fig. S7 in Supporting information). Here, tumor associated macrophages (U937), tumor cells (A549) and normal cells (LX-2) were used as model. FDA/PI double staining assay showed that the operation of insertion and withdrawn from the chamber had no effect on the cell viability (Fig. 4A). Next, TNF-α released by cells was monitored *in situ*. The ICR ratio of PET-Au-SuperDNA gradually increased over time toward cells with the density of 8×10^5 cells/mL, indicating continuous TNF-α secretion by the different cells and different secreted rate of different cells could be monitored (Fig. 4B). Besides, a linear correlation ($R^2 = 0.99$) between the results from our platform and commercial ELISA kit for TNF-α was obtained, validating the accuracy of the platform for TNF-α quantitative detection (Fig. 4C).

Intercellular communication between tumor associated macrophages (TAMs) and tumor cells is crucial for tumor development, metastasis, and related immune process. As reported, the continuous secretion of TNF-α by TAMs at low doses would induce epithelial mesenchymal transformation (EMT), which is a complex reprogramming process of epithelial cells, playing an

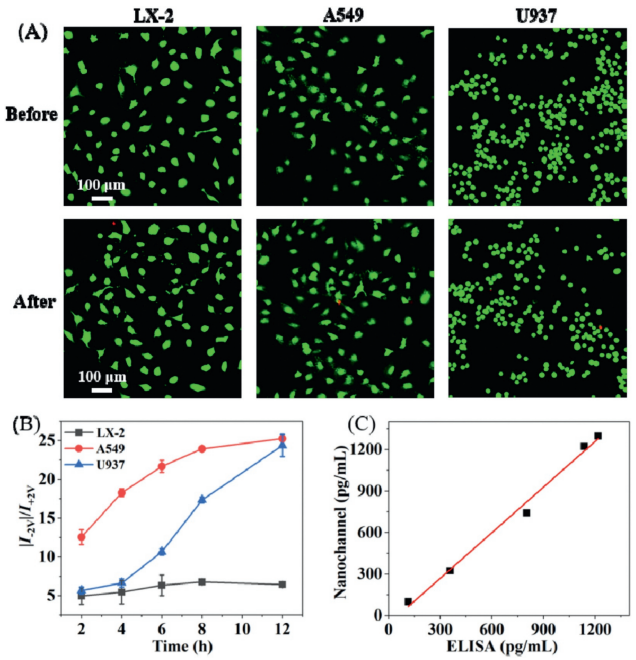

Fig. 4. (A) The merged CLSM images of cells stained by commercial fluorescence probe FDA (green/live) and PI (red/dead) before and after the operation of insertion and withdrawn from the chamber. (B) The ICR ratio *vs.* the secretion time with LX-2, A549 cells and M1 macrophages derived from U937 cells in the left chamber. (C) Accuracy verification of the proposed platform.

important role in tumor invasion and metastasis [35-37]. Our work will mainly investigate whether TNF-α has an effect on EMT. Tumor associated macrophages (U937) and tumor cell (BxPC-3) were used as model, they were cultured on the PET membrane, then rolled up and inserted into the left and right chamber of the self-made device, respectively (Fig. S8 in Supporting information). U937 cells were transformed into M0 macrophages after the incubation of Phorbol 12-myristate 13-acetate (PMA) of 24 h (Fig. S9 in Supporting information), then M0 macrophages were transformed into M1 macrophages to secret TNF-α under the stimulation of LPS. As shown in Fig. 5A, with the extension of LPS stimulation time, the $|I_{-2V}|/I_{+2V}$ was increased compared with the control group due to gradual secretion of TNF-α. Then the effects of TNF-α secretion on BxPC-3 cells were studied. Under immunofluorescence characterization, we found that the expression of EMT marker E-cadherin was down-regulated and the expression of vimentin was up-regulated (Fig. 5B) [38,39]. Western blot further revealed the significant changes in the protein levels

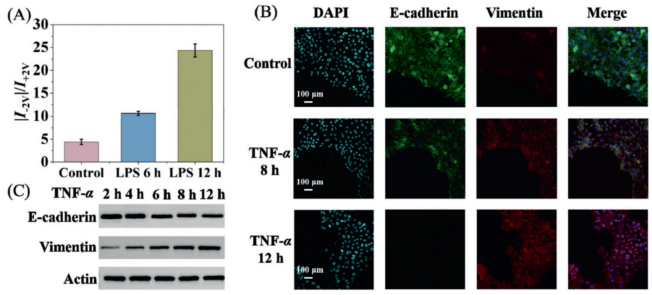

Fig. 5. Intercellular communication analysis. (A) The $|I_{-2V}|/I_{+2V}$ of PET-Au-SuperDNA after the treatment of LPS with different times. (B) Immunofluorescence micrographs of EMT markers (epithelial marker E-cadherin (green) and mesenchymal marker vimentin (red)) on BxPC-3 cells. Cell nuclei were stained with 4′,6-diamidino-2-phenylindole (DAPI, blue). (C) Western blot analysis of the protein expression of the EMT markers.

of E-cadherin and vimentin at different incubation time (Fig. 5C). These demonstrated that TNF-α induced BxPC-3 cells to achieve a transition from epithelial phenotype to mesenchymal phenotype, a kind of intercellular communication.

In summary, we have successfully fabricated SuperDNA self-assembled conical nanochannel (PET-Au-SuperDNA) through hybridization chain reaction (HCR). Based on self-made device, two functions were achieved: (1) Online detecting tumor associated macrophages (differentiated U937) released TNF-α, which opened the SuperDNA structure in the nanochannel. Through monitoring the ion current change, living cells released TNF-α could be *in situ* and noninvasive detected, a detection limit of 0.23 pg/mL and linear detection range was 0.1–1250 pg/mL was obtained. (2) Studying intercellular communication between tumor associated macrophages (U937) and tumor cells (BxPC-3). TNF-α induced epithelial-mesenchymal transformation of BxPC-3 cells, which confirmed by down-regulated EMT marker E-cadherin and up-regulated vimentin. The proposed nanochannel had high sensitivity, good specificity and repeatability, providing a new avenue for *in situ* analysis of cellular secretions and the study of intercellular communication.

Declaration of competing interest

The authors declare that they have no known competing financial interests or personal relationships that could have appeared to influence the work reported in this paper.

CRediT authorship contribution statement

Weiwei Liu: Methodology. **Yu Liu:** Investigation. **Zhaoyan Tian:** Formal analysis. **Zhaohan Wang:** Software. **Hui Liu:** Software. **Songqin Liu:** Funding acquisition. **Yafeng Wu:** Project administration.

Acknowledgments

This work was supported by National Natural Science Foundation of China (Nos. 22174016, 22374019, and 22209025), and Natural Science Foundation of Jiangsu Province (No. BK20220799).

Supplementary materials

Supplementary material associated with this article can be found, in the online version, at doi:10.1016/j.cclet.2024.110561.

References

[1] D.J. Kloosterman, L. Akkari, Cell 186 (2019) 1627–1651.
[2] A. Mantovani, P. Allavena, F. Marchesi, et al., Nat. Rev. Drug Discov. 21 (2022) 799–820.
[3] C. Song, D. Gao, T.Y. Yuan, et al., Chin. Chem. Lett. 30 (2019) 1038–1042.
[4] O.A. Sukocheva, M.E. Neganova, Y. Aleksandrova, et al., Cell Commun. Signal. 22 (2024) 251.
[5] P. Szlosarek, K.A. Charles, F.R. Balkwill, Eur. J. Cancer 6 (2006) 745–750.
[6] Z.Y. Tian, X. Qin, F.Y. Shao, et al., Chin. Chem. Lett. 34 (2023) 107656.
[7] J.Q. Fan, Y. Fan, Z.J. Wei, et al., Chin. Chem. Lett. 31 (2020) 1787–1791.
[8] R. Fontana, A. Mestre-Farrera, J. Yang, Annu. Rev. Pathol. Mech. 19 (2024) 133–156.
[9] P. Zhao, J. George, B. Li, et al., ACS Appl. Mater. Interfaces 9 (2017) 32482–32488.
[10] J. Gao, X.H. Zhu, Y. Long, et al., Anal. Chem. 96 (2024) 1795–1802.
[11] M. Genin, F. Clement, A. Fattaccioli, et al., BMC Cancer 15 (2015) 577.
[12] W.B. Tao, N.B. Xie, Q.Y. Cheng, et al., Chin. Chem. Lett. 34 (2023) 108243.
[13] G.W. Sun, W.L. Liu, J.H. Liu, et al., Atom. Spectrosc. 44 (2023) 392–400.
[14] Q. Xing, C. Vogt, K.W. Leong, et al., Adv. Funct. Mater. 24 (2014) 3027–3035.
[15] I.G. Reddin, T.R. Fenton, M.N. Wass, et al., Pharmacol. Res. 188 (2023) 106671.
[16] P.C. Gao, D.G. Wang, C. Che, et al., Nat. Protoc. 16 (2021) 4201–4226.
[17] G.W. Lu, N.Y. Lin, Z.J. Chen, et al., Chin. J. Chem. 41 (2023) 1374–1384.
[18] J. Zhang, C. Li, X. Zhi, et al., Anal. Chem. 88 (2016) 1294–1302.
[19] Y. Huang, L.X. Liu, C.H. Luo, et al., Chem. Soc. Rev. 52 (2023) 6270–6293.
[20] Q. Wang, X.D. Wang, M. Xu, et al., Chin. Chem. Lett. 30 (2019) 1557–1564.

[21] Y. Wang, X. Zhang, L. Zhao, et al., Biosens. Bioelectron. 98 (2017) 386–391.
[22] X. Yan, Y. Song, C. Zhu, et al., ACS Appl. Mater. Interfaces 8 (2016) 21990–21996.
[23] H.Y. Wang, Y.F. Ruan, L.B. Zhu, Angew. Chem. Int. Ed. 60 (2021) 13244–13250.
[24] W.R. Ma, L.L. Liu, Z.Y. Jiang, et al., Anal. Chim. Acta 1307 (2024) 342630.
[25] H. Hong, X. Lei, J.T. Wei, et al., Adv. Electron. Mater. 10 (2024) 2300782.
[26] C. Wei, A.J. Bard, S.W. Feldberg, Anal. Chem. 69 (1997) 4627–4633.
[27] R. Karnik, C. Duan, K. Castelino, et al., Nano Lett. 7 (2007) 547–551.
[28] G. Laucirica, M.E. Toimil Molares, C. Trautmann, et al., ACS Appl. Mater. Interfaces 12 (2020) 28148–28157.
[29] N. Qiao, Z.Q. Li, Z. Zhang, et al., Anal. Chim. Acta 1278 (2023) 341724.
[30] W.Q. Zhang, Y.D. Tu, H. Liu, et al., Angew. Chem. Int. Ed. 63 (2024) e202316434.
[31] X. Wang, J. Wu, R. Lv, et al., Anal. Chem. 94 (2022) 6234–6241.
[32] J. Wang, R. Fang, J. Hou, et al., ACS Nano 11 (2017) 3022–3029.
[33] P.C. Gao, Q. Ma, D.F. Ding, et al., Nat. Commun. 9 (2018) 4557.
[34] N.N. Liu, Y.N. Jiang, Y.H. Zhou, et al., Angew. Chem. Int. Ed. 125 (2013) 2061–2065.
[35] A. Oh, M. Pardo, A. Rodriguez, Cell Commun. Signal 21 (2023) 291.
[36] H. Zelová, J. Hoek, Inflamm. Res. 62 (2013) 641–651.
[37] D. Zhang, H. Yang, X.L. Dong, et al., Front. Immunol. 13 (2022) 854995.
[38] M.A. Huber, N. Kraut, H. Beug, Curr. Opin. Cell Biol. 17 (2005) 548–558.
[39] Y. Kang, J. Massagué, Cell 118 (2004) 277–279.